Chapter 20

Generative Biophysical Modeling of Dynamical Networks in the Olfactory System

Guoshi Li and Thomas A. Cleland

Abstract

Generative models are computational models designed to generate appropriate values for all of their embedded variables, thereby simulating the response properties of a complex system based on the coordinated interactions of a multitude of physical mechanisms. In systems neuroscience, generative models are generally biophysically based compartmental models of neurons and networks that are explicitly multiscale, being constrained by experimental data at multiple levels of organization from cellular membrane properties to large-scale network dynamics. As such, they are able to explain the origins of emergent properties in complex systems, and serve as tests of sufficiency and as quantitative instantiations of working hypotheses that may be too complex to simply intuit. Moreover, when adequately constrained, generative biophysical models are able to predict novel experimental outcomes, and consequently are powerful tools for experimental design. We here outline a general strategy for the iterative design and implementation of generative, multiscale biophysical models of neural systems. We illustrate this process using our ongoing, iteratively developing model of the mammalian olfactory bulb. Because the olfactory bulb exhibits diverse and interesting properties at multiple scales of organization, it is an attractive system in which to illustrate the value of generative modeling across scales.

Key words Generative model, Compartmental model, Olfactory bulb, Subthreshold oscillations, Network, Gamma oscillations

1 Introduction

Computational models of neurons and neural systems are constructed for many different reasons, from sharply defined proofs of concept to the instantiation of intricate working hypotheses. Some models emphasize the roles of the membrane and/or cable properties of individual neurons; others are constructed of highly simplified neurons in order to efficiently test or illustrate the capacities of functional network architectures. Similarly, some models are largely independent of specific experimental data, emphasizing the theoretical capacities of hypothetical systems or circuits, whereas others hew closely to parameters and response profiles estimated via

Fabio Marques Simoes de Souza and Gabriela Antunes (eds.), *Olfactory Receptors: Methods and Protocols*, Methods in Molecular Biology, vol. 1820, https://doi.org/10.1007/978-1-4939-8609-5_20,

experiment. Each of these approaches can be appropriate for addressing particular scientific questions.

Generative, multiscale biophysical models of neuronal networks are among the most complex computational model architectures commonly constructed. They are highly dependent on experimental data and generally cannot be usefully attempted until sufficient data exist to adequately constrain model parameters. Biophysical models employ equations that directly model physical and chemical processes in order to construct larger-scale models of the interactions among these processes. For example, a biophysical model of a neuron may include equations for the resistive and capacitative properties of the cell membrane (an insulating lipid bilayer separating two conductive aqueous media), equations describing the states, transition kinetics, conductances, driving forces, gating properties, and selectivities of transmembrane ion channels (including voltage-dependent and ligand-gated channels of multiple types), equations for the decline of voltage differentials along an extended neurite (cable theory), and equations describing intercellular signaling via electrical and chemical synapses. The dozens to hundreds of parameters typical of such models must be given values that enable the whole interconnected system, as well as its component parts, to reflect the properties of the system being modeled.

Generative models are those that are designed to generate appropriate values for all variables in the model, rather than (for example) driving certain properties or functions from a "black box" in order to study other phenomena more efficiently. For example, the membrane potential in a generative biophysical model of a neuron should not be directly assigned, but should be an outcome of the electrochemical balance of open channel conductances, which in turn are outcomes of the ionic selectivities of identified channel types as well as the states of their gating variables, which often depend in turn upon the membrane potential. Importantly, each of these individual variables is meaningful within the model, and reflects its biological counterpart. For example, increasing the membrane input resistance in such a model should increase the cable-theoretic length constant. Increasing the potassium concentration in the extracellular medium surrounding a typical neuron should depolarize its membrane potential. What will happen to the response properties of a given neuron when the hyperpolarization-activated cation current is blocked? What will happen when its intracellular calcium levels are strongly buffered? Generative models, when adequately constrained by data, should be able to predict experimental outcomes, and thereby serve as test beds for designing new experiments.

Most generative biophysical models are to some extent multiscale. The more explicitly multiscale models emphasize their generative properties across scales, from intracellular calcium

dynamics to cellular response properties, dendritic integration, matrices of synaptic connectivity, and the emergent properties of heterogeneous neuronal networks. In such models, nontrivial properties at each scale reflect the features of the biological system, such that the contributions of molecular properties to large-scale system functionality can be reasonably assessed within the model. Accordingly, such models are powerful tools for experimental design.

We here outline a general strategy for the design and implementation of generative, multiscale, biophysical models of neural systems that contribute meaningfully to the iterative process of scientific inquiry. We illustrate this process using our ongoing, iteratively developing model of the olfactory bulb (OB). Because the OB exhibits diverse and interesting properties at multiple scales of organization, it is an attractive system in which to illustrate the value of generative modeling across scales.

2 Model Conception

2.1 Establish Model Design and Purpose

The neuronal and circuit properties of the OB network have been well characterized over generations of study using a great diversity of experimental techniques, rendering it a particularly rich system for generative biophysical modeling. These studies have highlighted a number of "unusual" cellular and circuit properties in the OB that diverge from canonical forms and hence have attracted further study. Among these, for example, are action potential initiation in primary dendrites [1], somatofugal spike propagation in secondary dendrites, and a triune synapse in which direct excitation and indirect inhibition via the interposed spines of interneurons are evoked by the same afferent input and converge together onto principal neuron dendrites [2, 3]. Other specialized neurophysiological phenomena studied in the OB also have been observed and studied in other areas of the brain—for example, intrinsic subthreshold dynamics in principal neurons (discussed in [4]) and the evocation of local field potential oscillations, particularly the interplay between the theta and beta/gamma bands, in hippocampus (reviewed in [5]). While it is possible that the OB is genuinely atypical owing to its adaptation to the particulars of the olfactory modality—and it certainly exhibits some unique architectural properties—it is arguably more likely that some of these features simply have become evident in the OB because of the intensity of investigation. In other words, important noncanonical properties are likely to emerge in most brain circuits given further study. This prediction highlights two essential principles of generative modeling: (1) model design must be, to the extent possible, open to future elaborations without disrupting the foundational principles on which the model is based, and (2) the

process by which cellular and network parameters are reduced (simplified) during model construction is critical, and must be carefully considered.

2.2 Cellular and Network Properties of the Olfactory Bulb

The OB is the first center of synaptic integration in the olfactory system (reviewed by [6]). The axons of primary olfactory sensory neurons (OSNs) converge onto the surface of the olfactory bulb, with the axons of OSNs expressing the same odorant receptor type (out of a library of hundreds depending on species) converging together to form discrete bundles of arborized axonal neuropil called glomeruli (Fig. 1). Odorant receptors have reasonably broad chemoreceptive fields, such that odor specificity is encoded in replicable patterns of activation distributed across a substantial number of receptors and their associated glomeruli. The locations of glomeruli associated with particular receptors are substantially conserved among conspecifics, but their physical proximity on the OB surface

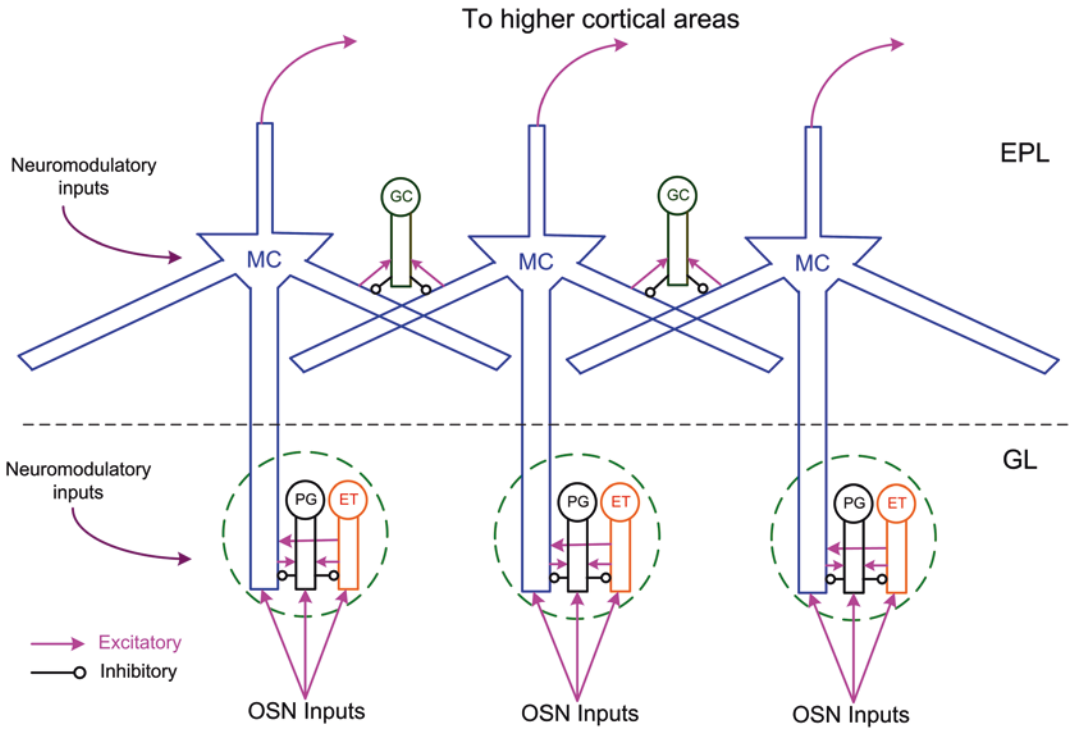

Fig. 1 The structure of the olfactory bulb. Primary olfactory sensory neurons (OSNs) expressing the same type of odorant receptor converge onto common glomeruli. Within a glomerulus, OSN axons synapse with the apical dendrites of mitral cells (MC) and two types of juxtaglomerular cells: periglomerular/superficial short-axon cells (PG) and external tufted cells (ETs). PG cells make dendrodendritic connections with MC apical dendrites and ET cell dendrites within glomeruli; ET cells excite MCs and probably mediate a substantial fraction of the afferent input delivered to MCs. In the external plexiform layer (EPL), granule cells (GCs) form reciprocal dendrodendritic synapses with MC lateral dendrites. Olfactory information then is conveyed to higher cortical areas via MC axons. *GL* glomerular layer, *EPL* external plexiform layer

is unrelated to their chemoreceptive fields ([7]; discussed in [8]). Activity in these glomeruli is sampled by principal neurons (mitral and tufted cells) and by juxtaglomerular interneurons (specifically, glutamatergic external tufted (ET) cells and a heterogeneous population of GABAergic and dopaminergic periglomerular/superficial short-axon (PG/sSA) cells) that mediate computations within each glomerulus and across glomeruli in the deep portion of the glomerular layer. These circuits effect a high-dimensional contrast enhancement operation that is analogous to that mediated by (two-dimensional) lateral inhibition in the retina [9] and regulated by cholinergic neuromodulation [10], and also a global feedback normalization operation that underlies concentration tolerance in the olfactory system [11, 12]. Notably, this normalization effect is considerably stronger in mitral than in tufted cells [13].

Deep to the glomerular layer (in mammals), laterally projecting dendrites in mitral and tufted cells support spike propagation and extend for essentially the full functional circumference of the OB. Reciprocal synapses with GABAergic granule cells along these dendrites effect lateral inhibition onto other principal neurons, though the most strongly weighted lateral synaptic interactions do not necessarily arise from neighboring columns, but are largely independent of proximity, indicating a distributed rather than a nearest-neighbor topology [14]. Moreover, these weights are likely to be plastic; the olfactory bulb exhibits substantial functional plasticity, including plasticity associated with adult neurogenesis [15, 16]. The strengths of these synaptic interactions, and their capacity to influence spike timing, also are effectively modified by cholinergic neuromodulation [17–19].

Afferent activation of the olfactory bulb evokes synchronous gamma-band local field potential (LFP) oscillations that are generated primarily by these reciprocal MC-GC synaptic interactions [20–24], with functional contributions by the intrinsic subthreshold dynamics of mitral cells [25, 26]. These LFP oscillations evince broadly coordinated driver potentials in OB neurons and the regulation of spike timing. Indeed, synaptic inhibition in this deep layer is likely to affect the timing, rather than the existence, of principal neuron action potentials (discussed in [8]; [26]), suggesting a common clock for coordinating the spiking activity exported to other regions of the brain. These gamma oscillations transition to a lower (beta) frequency during bidirectional interactions with piriform cortex [27, 28], and are embedded within theta-band oscillations that can be directly driven by respiration but may also be supported by the intrinsic theta-band rhythmicity of ET cells [29]. Notably, ET cells may be the primary source of mitral cell excitation; mounting evidence indicates that ET cell neurites are interposed between afferent fibers and mitral cell dendrites, as well as interacting with other juxtaglomerular interneurons in the glomerular layer network [12, 30–32].

In short, the OB exhibits a wide variety of physiological and dynamical properties spanning a range of physical and temporal scales. Building a generative biophysical model that faithfully incorporates all of these properties such that model manipulations can usefully predict experimental results is a complex task that is best performed iteratively. This implies, of course, that early iterations of the model must be both extensible and scientifically meaningful despite being substantially incomplete. We here describe our process for the iterative development of a generative biophysical model of the mammalian olfactory bulb [19, 26].

2.3 Principles of Generative Modeling

The first principle of iterative generative modeling is that a manageable present goal must be set for a particular project, while also keeping in mind the requirements of projected future goals. Specifically, each iteration requires a focused scientific question, or a set of related questions, that generates new, testable hypotheses. There must be sufficient experimental data, drawn from multiple scales of organization, to constrain the model such that any emergent properties of interest are likely to reflect reality. More complex models require a correspondingly greater amount and wider range of constraining data in order to meet this standard, providing an additional reason to keep each model iteration as compact as is reasonable.

In addition to limiting the scope of each iteration, it is usually necessary to limit the numbers of equations and parameters in the model, requiring a strategic reduction of the complexity of parts of the model design. This is partially due to the limitations of available computational power, but also because every free or partially free parameter adds degrees of freedom to the operation of the full model. Higher degrees of freedom can require more parameterization effort, but more importantly they also can reduce the likelihood that an apparent solution will be truly generative. That is, including too many underconstrained variables can permit fits to data that arise for spurious reasons that do not resemble the properties of the system being modeled. The solution is to allocate a limited budget of complexity to the core principles being explored in the current iteration of the model, while reducing other features in a manner that facilitates their later expansion.

Typical model reductions include reducing the numbers of neurons, reducing the compartmentalization of individual neurons, simplifying calcium dynamics, and omitting cell types that are hypothesized to serve little purpose within the scope of the present iteration of the model. Each of these simplifications has consequences. In multiscale models, for example, reductions in network size nearly always require deviations from measured experimental parameters because different properties of the network do not scale similarly. For example, reducing an interconnected network of a million neurons to a model network of 400 neurons will radically reduce the absolute number of synapses innervating any given

neuron. The individual synaptic weights then must be increased in order to generate appropriate postsynaptic currents under normal activity levels, thereby deviating from the experimentally measured values of individual cell-to-cell synaptic weights. Alternatively, the density of interconnections could be increased, but this then will have consequences for network function—for example, a highly interconnected network may become unable to generate a traveling wave of activity, if that is the biological phenomenon to be simulated. Determining appropriate scaling strategies is essential.

Finally, of course, the utility of generative models is to make experimentally testable predictions. Models that replicate experimental data but do not usefully predict further outcomes are of limited utility. This implies that models will sometimes extend markedly beyond what current experimental data support, presenting hypotheses with unclear bases in experiment. Certainly some such models are largely fanciful, or proofs of concept that serve other purposes in theoretical neuroscience. However, generative models also engage in this projective prediction. This may occur, for example, when a number of disparate model constraints at different levels of organization substantially reduce the range of possibilities beyond what may be intuitively obvious. That is, either an apparently projective prediction must be true, or a substantial portion of the model is wrong. Another example is when the generative model makes a strong prediction at one level of analysis, but not necessarily at others. A prediction at a weakly predicted level may be ruled out by subsequent experiments without disrupting the corresponding strong prediction. For example, the high-dimensional nontopographical contrast enhancement (NTCE) model for glomerular-layer contrast enhancement made the strong prediction at Marr's algorithmic level [33] that there must be global feedback normalization in the deep glomerular layer, maintaining a roughly consistent level of activation among mitral cells in response to odors presented at different concentrations [9]. Indeed, this was a known property of mitral cell response profiles across concentrations [34–36], though the mechanism was unclear. Based on contemporary anatomical and neurophysiological data (superficial short-axon cells being excitatory and having a mixed profile of projection distances; [37]), a weakly predicted implementational-level algorithm was developed that mediated this global feedback normalization effectively [38]. Subsequent experimental data revealed, however, that superficial short-axon cells actually project extensively across the glomerular layer, and are GABAergic and dopaminergic rather than glutamatergic; indeed, they are probably best considered as a single heterogeneous cell type together with periglomerular cells, hence their depiction herein as PG/sSA cells. It subsequently was conclusively demonstrated that PG/sSA cells do indeed effect global feedback inhibition across the deep glomerular layer (confirming the strong

algorithmic prediction) but via direct, distributed GABAergic/dopaminergic projections rather than by the predicted mechanism (rejecting the weak implementational prediction) [12]. Consequently, subsequent iterations of the generative model must correct this error in implementation, but the critical algorithmic properties of that deep glomerular layer circuit, upon which major features of the model depend, now enjoy direct experimental support.

We now briefly describe the concrete implementation of our present OB model iterations [19, 26], noting in particular the local goals of these two iterations and decisions that were made to facilitate future model development. We first briefly cover the general process of compartmental modeling, which is more extensively addressed elsewhere (e.g., [39–41]). We omit direct discussion of the earlier iterations preceding these general models, e.g., the glomerular circuit models of nontopographical contrast enhancement and its cholinergic neuromodulation [9, 10] and the cellular models of mitral cell intrinsic dynamics [42] and periglomerular cell diversity [43].

3 Methods

3.1 General Framework of Biophysical Neuronal Models

Most biophysical neuronal models are conductance-based compartmental models that contain Hodgkin-Huxley-type ionic currents, cable properties, and dynamics derived from experimental data. The standard approach is to discretize the neuron into a finite number of interconnected anatomical compartments, each of which comprises a single state for each variable (i.e., a compartment has a single membrane potential, a single calcium concentration, a single state for each gating variable of each ionic conductance, etc.). Importantly, one can accurately model the membrane potential at the end of a long cable (dendrite) without requiring that dendrite to have many compartments; however, the number of compartments does determine the spatial resolution of the voltage decline along such an extended cable. The schematic of an equivalent circuit for a generic compartmental model is shown in Fig. 2. Generally, each compartment expresses a membrane capacitance (C_m), a passive leakage current (a fixed resistance R_m associated with a battery E_m), and a number of active ionic currents (a variable conductance G_i associated with a battery E_i). These batteries define the reversal potentials of their respective currents, reflecting their permeant ions. Based on the equivalent circuit (Fig. 2), we can obtain the current balance equation for a representative compartment:

$$c_m \frac{dV_m}{dt} = \frac{(E_m - V_m)}{R_m} + \sum_i G_{ci}(E_{ci} - V_m) + \frac{(V_m' - V_m)}{R_a} + \frac{(V_m'' - V_m)}{R_a} \quad (1)$$

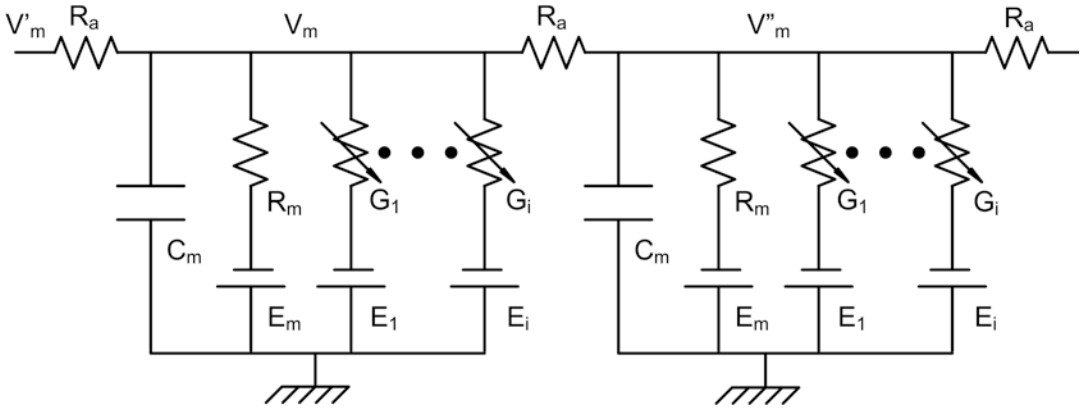

Fig. 2 Equivalent electrical circuit for two connected generic neural compartments. The membrane potentials V_m, $V_m^{'}$ and $V_m^{''}$ are associated with each individual, isometric neural compartment. C_m is the membrane capacitance, R_m the membrane resistance, R_a the axial resistance, and E_m the leakage reversal potential. Subscripts 1…*i* denote *i* different active (variable) conductances and their associated reversal potentials (e.g., conductances G_1, G_2, etc., with reversal potentials E_1, E_2, etc.). Conductances G_i are regulated by gating variables, which may depend on membrane voltage and/or the presence of activating ligands

where V_m is the membrane voltage, R_a is the axial resistance, and $V_m^{'}$ and $V_m^{''}$ are the voltages of the two adjacent compartments. A multicompartmental model will consist of a number of coupled equations of the form of Eq. 1 [44].

Active transmembrane ionic conductances are usually modeled using the Hodgkin-Huxley formalism [45]. Specifically, the conductance of a membrane channel *i*, G_i, is modeled as:

$$G_i = g_i m^p h^q \tag{2}$$

where g_i is its maximal conductance density, m its activation gating variable (with exponent p), and h its inactivation gating variable (with exponent q). The kinetic equation for the gating variable x (m or h) satisfies a first-order kinetic model,

$$\frac{dx}{dt} = \phi_x \frac{x_\infty(V) - x}{\tau_x(V)} \tag{3}$$

where ϕ_x is a temperature-dependent factor, $x_\infty(V)$ is the voltage-dependent steady state, and $\tau_x(V)$ is the voltage-dependent time constant. Equivalently, Eq. 2 can be written as:

$$\frac{dx}{dt} = \phi_x \left(\alpha_x(V)(1-x) - \beta_x(V)x\right) \tag{4}$$

where $\alpha_x(V)$ and $\beta_x(V)$ are the voltage-dependent rate constants. The parameter values for the rate constants α_x and β_x, steady state x_∞, and time constant τ_x of the gating variables determine the mod-

el's dynamical properties and are typically based on cellular electrophysiological measurements (e.g., from voltage clamp or current clamp experiments).

3.2 Olfactory Bulb Model Design Goals

We sought to construct a general OB model that would generatively exhibit intrinsic, activity-gated gamma oscillations that shaped mitral cell spike timing. Importantly, the oscillations were to be emergent properties of data-constrained mitral-granule cell interactions within the external plexiform layer (EPL), arising from their intrinsic cellular and synaptic properties rather than being directly driven. The model also embedded glomerular-layer computations such as NTCE, though for computational efficiency the costly global feedback normalization process was omitted, requiring odorant stimuli to all be presented at similar intensity levels. To provide a broader base of constraining data, the first of these iterations emphasized the effect of cholinergic neuromodulation (both nicotinic effects in the glomerular layer and muscarinic effects in the EPL) on OB operation [19]. The second was developed in concert with new experimental data and emphasized the origin and dynamical basis for gamma oscillations, including the respective contributions of EPL network properties and the intrinsic membrane dynamics of mitral cells [26], and the capacity of these oscillations to maintain negligible phase lag across the entire EPL [46]. These models consequently required dynamically accurate mitral cells, glomerular layer PG/sSA interneurons, and granule cell interneurons, as well as the appropriate synaptic connectivity. External tufted cells, projecting tufted cells, and deep short-axon cells were omitted, but are scheduled for inclusion in future iterations of the model.

3.3 Implementation of Cellular Models

3.3.1 Cellular Morphologies and Compartmentalization

After establishing design goals for the model, and considering the appropriate complexity of the different model elements, the next step is to determine the morphological and physiological properties of each class of neuron to be represented. Neurons in biophysical models are rarely single-compartment "point" neurons, but rather comprise a number of interconnected sections corresponding to physical elements such as soma, axon and dendrites, each of which may comprise one or more—sometimes many more—isometric compartments. Examples of the basis for determining the appropriate complexity and compartmentalization of model neurons for particular model goals follow.

Mitral cells (MCs). MCs have a long primary dendrite ending in a glomerular tuft that receives excitatory afferent synaptic inputs [47], and extensive lateral (secondary) dendrites that synaptically contact granule cell dendrites across the functional extent of the external plexiform layer [48]. Our MC model neurons were comprised of a soma, a lateral dendrite, an apical dendrite, and a glomerular tuft at the distal end of the apical dendrite [19]. The axon, which emerges from the base of the cell body [48], was omitted.

Each spatially extended section was divided into a number of isopotential compartments depending on the spatial resolution and the desired space constant or electrotonic length of a particular section. For instance, the soma and tuft were each modeled as single compartments, whereas the apical dendrite was modeled using five compartments to electrotonically separate the spike-generating regions of the dendrite and soma from the afferent synaptic input location in the tuft [47]. The long lateral dendrite was divided into seven compartments in order to model realistic spike propagation along the long lateral dendrite and assess the dynamical interactions between the locations of inhibitory synapses and spike propagation [49]. Other biophysical models of MCs contain different numbers of compartments, depending in part on the goals of the study in question [42, 50–53]. Generally, the number of compartments to implement depends on several factors, including (1) the electrotonic length of the neuronal section in question, which depends on its length, diameter, total membrane conductance, and axial resistivity, (2) the desired spatial resolution (i.e., at how many points along the length of the section will its properties need to be measured?), (3) the available computational resources, as more compartments and mechanisms require more simulation time; and, of course, (4) the requirements of the scientific problem being investigated.

One critical property of mitral cells that required careful model development is their resonance. Mitral cells display intrinsic subthreshold membrane potential oscillations (STOs) at frequencies ranging from 10 to 50 Hz depending on the mean membrane potential [25]. These STOs can constrain the precise timing of action potential generation, and their phases can be reset by inhibitory synaptic inputs. They also have been suggested to play a critical role in OB gamma oscillations [53], though our models suggest that their role in OB network gamma is somewhat more subtle [26].

Periglomerular/superficial short-axon (PG/sSA) cells: As described above, PG/sSA cells are heterogeneous in morphology, physiology, expression profiles, and connectivity; because the categories formed by these various differences do not correspond with one another, separate cell classes cannot be clearly defined (discussed in [43]). Morphologically, PG cells have from one to three relatively thick primary dendritic shafts leading to thinner branches that ramify within a glomerulus and often (60%) exhibit spines (gemmules) [30]. Some PG/sSA cells receive excitation primarily from olfactory receptor neurons (PGo type), whereas others are excited primarily by external tufted (ET) cells (PGe type; [30, 54]). PG/sSA cells also can be divided into four subclasses based on intrinsic response properties, described as low-threshold spiking (LTS), adapting, nonadapting and irregular spiking [55], and can be further differentiated by their expression of calbindin, calretinin, and/or other molecules [56, 57]. Finally, the arborizations

of PG/sSA neurons vary from those that are restricted to one glomerulus, to those that innervate a small number of neighboring glomeruli, to those that project much more broadly [58], ultimately delivering inhibition across the full extent of the OB glomerular layer [12]. As the main purpose of PG/sSA cells in the current iterations of our model was to fulfill the NTCE function, we initially limited our PG/sSA implementation to the PGo form, reserving the more extensive lateral projections and their global normalization function for a subsequent model that also includes ET cells, their primary synaptic target. Accordingly, we implemented PG/sSA neurons using a soma, a single-compartment primary dendrite, a spine shaft, and a spine body, omitting the axon. Finally, we chose to include only LTS-generating PG/sSA cells, since this is the primary observed response profile of this cell class; non-LTS responses may be more associated with the broadly projecting sSA form [55], the feedback normalization function of which we omitted from the present iteration of the model.

Granule cells (GCs): GCs make a large number of inhibitory synaptic contacts with the lateral dendrites of MCs, via large spines that form reciprocal synapses with MC lateral dendrites [59]. Inhibitory synaptic transmission from GCs to MCs is thought to be graded since isolating GC spines from their somata does not impair gamma field oscillations [21], though GCs do spike sparsely [60], and effective lateral inhibition may require GC spikes owing to the biophysics of spine-spine interactions. Moreover, even though GC spikes are not required to activate graded inhibitory synapses, the dynamics of GC GABA release are still essentially pulsed because release is evoked by MC spikes. The morphological features of GCs include several basal dendrites within the vicinity of the cell body, and multiple thin (1–2 μm) and long (up to 600 μm) dendrites projecting to the EPL, wherein they synapse with the lateral dendrites of MCs [61].

As with PG/sSA cells, relatively simple GC models can be used, as their major function in the present model iteration is to provide feedback inhibition to MC lateral dendrites. (Models engaging spine-spine interactions, the respective roles of the perisomatically generated sodium spike and the dendritically generated calcium spike, and activity-dependent synaptic plasticity rules, for example, await future iterations). Reduced GC compartmental models meet these modest requirements with only a soma, a long basal dendrite, and one or more spines [19]. Table 1 shows the reduced compartmentalization (with dimensions) of our MC, PG/sSA and GC model neurons.

3.3.2 Cellular Membrane Mechanisms

The electrophysiological properties of neurons depend mainly on their cellular membrane and perimembrane mechanisms, including ion channel activity, membrane transport, and calcium dynamics, as well as on the physical distributions of these mechanisms across

Table 1
Morphological parameter values and passive electrical properties of MC, PG/sSA (PG), and GC model cells (Li and Cleland [19])

Cell type	Section	Diameter (μm)	Length (μm)	C_m (μF/cm²)	R_m (Ω cm²)	R_a (Ω cm)	E_m (mV)
MC	Soma	20	25	1.2	30,000	70	−60
	Lateral dend	3.4	500				
	Apical dend	3.5	370				
	Tuft	0.5	20				
PG	Soma	8	8	1.2	20,000	80	−65
	Dend	1	100				
	Spine shaft	1	1				
	Spine body	1	1				
GC	Soma	8	8	2	30,000	70	−60
	Dend	1	150				
	Spine shaft	1	1				
	Spine body	1	1				

the different sections of each neuron type. The inclusion of particular ion channel species in each section (e.g., soma, dendrite) should be based on experimental data and physiological properties. For example, the most salient dynamical property of MCs is that they exhibit STOs, the frequency of which depends on the membrane potential [25, 48, 62]. Moreover, in response to excitatory input, MCs fire intermittent clusters of action potentials (APs) interspersed with long period of STOs, and there is a notable delay before generation of the first action potential [48, 62]. To replicate STOs, the MC model cell was endowed with a persistent sodium current I_{NaP} and a slowly inactivating potassium current I_{KS} [19, 42]. An inactivating potassium current I_A was included to model the delayed onset of firing. Additionally, the MC model cell included a regular fast sodium (I_{Na}) and a delayed rectifier potassium (I_{DR}) currents for spike generation, and a high-threshold Ca^{2+} current (I_{CaL}) together with a Ca^{2+}-dependent potassium current $I_{K(Ca)}$ to enable intermittent burst firing [19].

To model the LTS, the PG/sSA model cell contained a low-threshold Ca^{2+} current I_{CaT} [19], along with a hyperpolarization activated cation current (I_H) that enabled the generation of rebound burst firing upon the release of hyperpolarizing input [63]. The PG/sSA model cell also included a muscarinic M-current (I_M), based on the observation that muscarinic receptors are weakly expressed in the glomerular layer [64]. Finally, it contained the

Table 2
Distribution of active ionic currents in the MC, PG/sSA (PG), and GC model cells (Li and Cleland [19])

		I_{Na}	I_{NaP}	I_{DR}	I_M	I_A	I_{KS}	I_H	I_{CaL}	$I_{CaP/N}$	I_{CaT}	I_{CAN}	$I_{K(Ca)}$
MC	Soma	✓	✓	✓	–	✓	✓	–	✓	–	–	–	✓
	Lateral dend	✓	✓	✓	–	–	✓	–	✓	–	–	–	–
	Apical dend	✓	✓	✓	–	–	✓	–	✓	–	–	–	–
	Glom tuft	✓	✓	✓	–	–	✓	–	✓	–	–	–	–
GC	Soma	✓	–	✓	✓	✓	–	–	–	–	–	–	–
	Dend and spine	✓	–	✓	–	✓	–	–	–	✓	✓	✓	✓
PGC	Soma	✓	–	✓	✓	✓	–	–	–		–	–	–
	Dend and spine	✓	–	✓	–	✓	–	✓	–	✓	✓	–	✓

spike generation currents I_{Na} and I_{DR}, an inactivating potassium current I_A, a high-threshold Ca^{2+} current $I_{CaP/N}$, and a Ca^{2+}-dependent potassium current $I_{K(Ca)}$ [19].

One important property of GC action potential firing is that it produces after-hyperpolarization (AHP) responses following a train of action potentials. When muscarinic cholinergic receptors on GCs are activated, these AHPs are converted into after-depolarization (ADP) responses [17], extending the period of GABA release and thereby delaying the release of MCs from inhibition. The AHP responses are mediated by both a muscarinic M-current (I_M) and a Ca^{2+}-dependent potassium current $I_{K(Ca)}$, whereas the ADP responses are mediated by a Ca^{2+}- activated non-specific cation current I_{CAN} [17, 18]. GCs also exhibit a delayed onset of spike firing in response to weak current injection, suggesting the expression of an inactivating potassium current I_A [65]. Moreover, GCs contain both a low-threshold Ca^{2+} current I_{CaT} and a high-threshold Ca^{2+} current $I_{CaP/N,}$ as well as spike-generating fast sodium (I_{Na}) and delayed rectifier potassium (I_{DR}) currents [18]. Table 2 shows the distribution of active ionic currents in the different sections of our MC, PG/sSA, and GC model cells [19].

3.3.3 *Platforms for Model Implementation*

After determining the compartmental representation of each section of MC, PG and GC model cells, and the appropriate mechanisms (with suitable kinetic functions) and densities expressed in each, one can begin to implement these models using either general computing languages such as C/C++, MATLAB, and Python or specialized neuronal modeling packages such as NEURON [66], GENESIS [67], or MOOSE [68]. General computing languages have the advantage of being flexible and efficient, while specialized modeling packages provide streamlined functions and utilities to

greatly facilitate the implementation of biophysical models. The general procedure for implementing cellular models with specialized neuronal simulators includes specifying the cellular morphology, defining the kinetics of active ionic currents, and determining the inclusion and density of appropriate ionic currents and other mechanisms within each section or compartment.

3.3.4 Parameterization of Cellular Models

After a basic (unrefined) cellular model has been implemented, suitable parameters must be determined so that the model exhibits patterns of activity that reasonably and generatively reflect experimental data. Three major parameter types can be considered: morphological dimensions, passive parameters, and active parameters. Morphological dimensions are based on experimental measurements of neuronal anatomy (e.g., soma size, the lengths, diameters, and tapering of dendrites and axons). Estimated morphological parameters for MC, PG/sSA, and GC cells are shown in Table 1. Passive electrical properties include specific membrane capacitance (C_m), membrane resistance (R_m), axial resistivity (R_a) and leak current reversal potential (E_m). These parameters also should be based on experimental data; the estimated passive parameters of MC, PG/sSA and GC model cells are listed in Table 1 [19].

Active parameters correspond to the kinetics of active ionic channels, and include maximum channel conductances, gating variables (activation/inactivation, including both steady-state and time constant functions), ligand sensitivities (such as for intracellular calcium or extracellular neurochemicals), and intracellular Ca^{2+} release and buffering kinetics. Ideally, these parameters also should be based on experimental data. However, such quantitative experimental details often are not available. If the kinetic equation of an ionic current is not known firsthand, it can be estimated from other mechanisms of the same type that are more fully described. After such baseline kinetic equations are established, the kinetic parameters then can be tuned so that the responses from MC, PG/sSA, and GC model cells correspond properly with experimental data. The most consequential adjustments of these commonly underdetermined parameters usually include altering the maximal conductance densities, shifting the steady-state activation and inactivation functions, and scaling the time constants.

Parameter estimation can be conducted both via hand-tuning and via automated/automation-assisted parameterization methods. Hand-tuning should be guided by associating specific parameters with particular firing patterns of the neurons to the extent possible. For example, we know that the persistent sodium current I_{NaP} and the slowly inactivating potassium current I_{KS} have been associated with the generation and maintenance of STOs. By tuning their maximal conductances and the time constants of their activation and inactivation variables, one can adjust both the amplitude and frequency of STOs to levels that match experimental

recordings [25, 48]. Automated parameterization involves establishing the response criteria to be matched (e.g., firing rates, burst frequencies, number of spikes in each burst, STO amplitude and frequency, adaptation levels, etc., each as a function of baseline membrane potential), and then selecting searching parameters with bounded ranges and using either brute-force simulations with post hoc assessment or automated iterative procedures to determine the optimal parameter sets that best satisfy the matching criteria. Commonly used iterative algorithms include conjugate-gradient descent, genetic algorithms, simulated annealing, and stochastic search [69], though additional methods are always under development (e.g., [70]).

Importantly, cellular-level parameter optimizations are likely to require further adjustment after instantiation of the larger network model, both to adapt to changes effected by new interactions (e.g., ongoing synaptic activity) and in order to allow network activity profiles to be optimized to better match experimental data at this larger scale. Hence, it is wise during cellular model optimization to take note of the parameter ranges and tolerances that generate acceptable outcomes, as opposed to determining a single optimized set of parameters. This practice will ease the task of determining parameter sets that reflect both cellular and network activity profiles properly and simultaneously.

3.4 Connect Cellular Models into a Functional Network

3.4.1 Determine the Size and Topologies of the Network

The first step to develop a functional network is to identify the network topology or topologies on which it is based. Most reasonably complex networks will have multiple interacting systems of connectivity; for example, in the OB, intraglomerular networks, the nonspecific feedback normalization interactions across the deep glomerular layer, and the specific, probably plastic matrix of interactions between MCs and GCs in the EPL each exhibit their own topological properties that often can be tuned separately before being united into a single larger network. Our OB models implemented these embedded topologies by incorporating both intracolumnar (e.g., PG/sSA-MC) and intercolumnar (MC-GC) computations [19, 26]. One of the goals governing the MC-GC interaction topology was to generate a diversity of distances between the MC soma and the location of MC-GC synaptic interaction, so that spike travel times would be appropriately heterogeneous and we could assess whether this was a hindrance to the maintenance of coherent gamma oscillations. In the earlier iteration, the locations of GC synapses were randomized along MC lateral dendrites [19], whereas in the subsequent iteration, an explicit two-dimensional spatial framework was constructed and each neuron and synapse located specifically thereon [26].

The size of the network should depend on the particular problem under investigation as well as the available computational resources. For most biophysical models, the size of the network is

usually several orders of magnitude smaller than the corresponding biological system owing to computational constraints. However, this does not preclude the generation of useful insights and information from the network model, because by scaling the synaptic densities and weights, a relatively small network will often be able to produce network behaviors similar to those of larger networks. (As noted above, such scaling typically will require that some network features, such as synaptic densities and weights, deviate from their measured experimental parameters because different properties of the network will not scale similarly.) The network size is often a parameter of interest, and the relative numbers of neurons of different classes should reflect those of the biological network, too, though the actual ratios may deviate substantially (in part owing to scaling issues). The importance of this principle of course will depend on the goals of the model. For example, the Li and Cleland (2013) model [19] includes 25 MCs, 25 PG/sSA cells, and 100 GCs for a total of 150 model cells; in this model, it was important that GCs substantially outnumber the number of OB glomerulus-associated columns (each comprising one MC and one PG/sSA cell), but it was not critical that the GCs outnumber the other cell types by orders of magnitude as they do biologically. Subsequent models including intraglomerular gap junction-based interactions among MCs will of course require multiple MCs per glomerulus; models including feedback normalization will include additional PG/sSA cells with more extensive lateral projection profiles and should incorporate ET cells as well. Designing generative models iteratively enables these additional sources of complexity to each be incorporated in turn, avoiding the geometric increases in the computational time required for parameterization that can arise when trying to optimize too many important parameters at once.

3.4.2 Select a Suitable Synaptic Model and Establish Synaptic Properties

There are two primary ways to model synaptic transmission between neurons. The first one is to approximate synaptic conductance change with a smooth function. For example, the smooth shape of the synaptic conductance can be approximated by an alpha function [71, 72]:

$$g_{\mathrm{syn}}(t) = g_{\max}\frac{t}{t_{\mathrm{p}}}e^{\left(1-t/t_{\mathrm{p}}\right)} \tag{5}$$

where $g_{\max}$ is the maximal synaptic conductance (that can be evoked by a single presynaptic spike; such values can be experimentally measured) and t_{p} is the peak time at which the conductance reaches its maximal conductance $g_{\max}$. A more general form of analytical expression is the double exponential function [67]:

$$g_{\mathrm{syn}}(t) = \frac{Ag_{\max}}{\tau_1-\tau_2}\left(e^{-t/\tau_1}-e^{-t/\tau_2}\right) \tag{6}$$

where A is a normalization constant chosen so that g_{syn} has the maximal value of g_{max}, and τ_1 and τ_2 are synaptic rise and decay time constants, respectively. In response to a presynaptic spike input, the synaptic conductance will increase to the peak value g_{max} with the time constant τ_1 and decay to zero with the time constant τ_2.

The major drawback of smooth function models is that they do not provide a natural saturation mechanism. In the presence of a train of presynaptic spike inputs, a synaptic conductance will build up substantially (exceeding g_{max} in the above definition) for slow synapses with a large decay time constant. In addition, smooth function schemes only apply to spike-mediated synaptic interactions (i.e., the synapse is activated by spike input); they cannot model graded synapses, in which the synaptic conductance depends on the presynaptic membrane voltage in a graded manner. Another way to model synaptic conductance is to use a first-order kinetic model [53, 73, 74]:

$$g_{syn} = g_{max} s \tag{7}$$

where the gating variable s represents the fraction of open synaptic ion channels and obeys first-order kinetics

$$\frac{ds}{dt} = \alpha F\left(V_{pre}\right)\left(1 - s\right) - \beta s \tag{8}$$

where α and β are the channel opening rate constants, and $F(V_{pre})$ is an instantaneous sigmoidal function of the presynaptic membrane potential V_{pre}:

$$F\left(V_{pre}\right) = 1 / \left(1 + \exp\left(-\left(V_{pre} - \theta_{syn}\right) / \sigma\right)\right) \tag{9}$$

The half-activation potential θ_{syn} and the gradedness parameter σ determine whether the synapse is spiking or graded. For spiking synapses, θ_{syn} is set to a relatively high value (e.g., 0 mV) and σ is relatively small (e.g., 0.2), such that the activation threshold is hard or steep. In contrast, for graded synapses, θ_{syn} is set to be below the spiking threshold (e.g., −50 mV) and σ is relatively large (e.g., 2) so the activation threshold is much softer. In our OB network models [19, 26], excitatory glutamatergic synapses were mediated by AMPA/NMDA receptors whereas the inhibitory synapses were mediated by $GABA_A$ receptors. We used spiking synapses for the AMPA/NMDA synapses and graded synapses for the GABAergic synapses (although, as noted above, their activity still was largely pulsed owing to their activation by MC spikes). The advantage of this first-order kinetic model is that it innately models synaptic saturation correctly and the peak synaptic conductance is clamped at g_{max}. That is, the g_{max} parameter directly represents the actual maximum conductance of the synapse (all channels open, all gating variables = 1), and hence by definition cannot be exceeded.

Regardless of the type of synaptic model, the synaptic time constants should be estimated based on experimental data, as they can be major determinants of network function. Synaptic currents I_{syn} are calculated as:

$$I_{syn} = W g_{syn}\left(V - E_{syn}\right) \tag{10}$$

where W is the synaptic weight, V is the current membrane potential of the compartment, and E_{syn} is the synaptic reversal potential. For AMPA/NMDA currents E_{syn} is around 0 mV, while for $GABA_A$ currents, E_{syn} is about −80 mV. The synaptic weight is a scaling factor that must be scaled properly so that a reduced network can generate realistic activity patterns matching those of the biological network, and also is modifiable for plastic synapses during learning. Odor learning in the OB depends on the modification of intrinsic synaptic weights [15, 75], as well as the incorporation of adult-born neurons [76, 77]. Note that although we varied synaptic weights systematically in our present OB model iterations to examine their impact on network dynamics [19, 26], we did not model synaptic plasticity explicitly. Implementation of synaptic plasticity will be critical in future iterations of the model to investigate how odor representations change with learning and experience [78, 79].

3.5 Network Simulation

3.5.1 Provide Inputs to the Network

Sensory systems generally need to receive external input to generate meaningful activity. There are two types of external inputs: random nonspecific background inputs and task-specific inputs (in the present context, odor input in the OB). Random background inputs represent both intrinsic and extrinsic sources of background noise and generate characteristic profiles of spontaneous network activity. In our OB model [19], all the neurons in the network received independent Poisson-distributed spike trains. In contrast, the afferent odor input was modeled by a sigmoidal function [53]:

$$I_{OSN} = u_0 + 0.5\left(u_s - u_0\right)\left[\tanh\left(\frac{3\left(t - t_{ORN}\right)}{r} - 3\right) + 1\right] \tag{11}$$

where u_0 is the preodor value and u_s the steady-state value after odor excitation. The parameter r determines the transition rate from u_0 to u_s and t_{orn} the time of odor onset. Periodic stimulation, replicating respiration or higher-frequency investigative sniffing, also can be effectively used. In either case, MCs and PG/sSA cells in independently tuned glomeruli received different levels of afferent input, simulating the differential activation of distinct receptor-associated glomeruli as a function of odor quality (Fig. 1). Similar profiles of receptor activation denoted correspondingly perceptually similar odorants.

3.5.2 Run Network Simulation

After the network is fully implemented, simulation parameters must be selected, including the integration method, integration timestep, and total simulation time. Chiefly, the integration timestep needs to be small enough to ensure the accuracy of simulation results; however, shorter timesteps require correspondingly greater computational resources. A rule of thumb is to progressively reduce the integration timestep until no significant difference in stimulus output is produced. Simulation data should be saved into files for subsequent analysis.

3.5.3 Parameter Fitting (Multiscale Criteria)

As with cellular simulations, the results of network simulations must reasonably replicate the network activity in the biological system. Common assessment criteria include spontaneous and odor-evoked firing rates in each neuron type, temporal firing patterns, LFP signals (extracellular potential changes generated by a group of neighboring neurons) and effects under neuromodulation. Significant discrepancies between the simulation results and experimental data suggest the need for further parameter fitting. Major network parameters include synaptic connection densities, synaptic weights, synaptic delays, and synaptic time constants. In some circumstances, some reparameterization of cellular models will be necessary in order to generate proper network level responses. Under such circumstances, as discussed above, the determination of parameter tolerances in cellular models to limit the range of acceptable parameters becomes particularly important. For example, the intrinsic STO frequency may constrain the gamma oscillation frequency of the OB network. After the network has been properly parameterized, the model then can be used to study a range of problems in olfactory information processing such as odor discrimination and recognition, mechanisms of LFP oscillations, and the effects of neuromodulation. In particular, insights and predictions from the model can be used to guide experimental design.

3.6 Visualization and Analysis of Simulation Data

Best practices for visualization and analysis of simulation data are to save the simulation data into files and then to visualize and analyze them using general computing languages such as MATLAB or Python. Common raw data visualizations include plots of membrane voltage traces of representative neurons, conductances of representative transmembrane currents and synapses, and spike raster plots of the whole network. Major network activity patterns can be visualized and quantified by perievent time histograms (PETH), firing rates, oscillation power and frequency, spike phase plots, and synchronization and oscillation indices. For oscillation analyses, a simulated local field potential (sLFP) can be constructed from any number of cellular timeseries and filtered within a certain frequency range. For example, we constructed a global sLFP by filtering the mean (somatic) membrane potentials across all MCs in the 2D OB network model [26]. Filtering was accomplished with a band-pass

filter (10–100 Hz) using the MATLAB functions FIR1 and FILTFILT. The frequency power spectrum of an sLFP can be obtained by a fast Fourier transform (FFT) of the filtered sLFP. The network oscillation frequency then can be estimated from the location of the spectral peak in the power spectrum. Other visualization and analysis methods also may be used depending on the scientific problems of interest.

3.7 Summary

In summary, the development of generative biophysical models of dynamical networks in the olfactory system involves clearly determining the design goals and the appropriate model complexity, implementing cellular models with parameter optimization, connecting cellular models into a functional network with further parameter fitting, and analyzing the simulation data. Generative model development is usually an iterative process with extensive parameter searching so that the network output comes to closely reflect existing experimental data. Partitioning long-term model plans into achievable steps is necessary to construct more complex generative models. Critically, each of these steps must be carefully conceived and adequately constrained by neurophysiological data, and embedded within a flexible, multiscale architecture to facilitate future model extensions. We here illustrate the development process of a generative, multiscale, biophysical model of the mammalian olfactory bulb [19, 26], which, owing to its diverse cell types, interesting circuit architectures, and intricate cellular and network dynamics, is a particularly rich platform for illustrating generative model design.

Acknowledgments

NIDCD grants R03 DC013872 to G.L., R01 DC014701 and R01 DC014367 to T.A.C.

References

1. Chen WR, Shen GY, Shepherd GM, Hines ML, Midtgaard J (2002) Multiple modes of action potential initiation and propagation in mitral cell primary dendrite. J Neurophysiol 88:2755–2764
2. Pinching AJ, Powell TP (1971) The neuropil of the glomeruli of the olfactory bulb. J Cell Sci 9:347–377
3. Shepherd GM, Greer CA (1998) Olfactory bulb. In: Shepherd GM (ed) The synaptic organization of the brain, 4th edn. Oxford University Press, New York
4. Skinner FK (2013) Moving beyond type I and type II neuron types. F1000Res 2:19
5. Colgin LL (2016) Rhythms of the hippocampal network. Nat Rev Neurosci 17:239–249
6. Nagayama S, Homma R, Imamura F (2014) Neuronal organization of olfactory bulb circuits. Front Neural Circuits 8:98
7. Soucy ER, Albeanu DF, Fantana AL, Murthy VN, Meister M (2009) Precision and diversity in an odor map on the olfactory bulb. Nat Neurosci 12:210–220
8. Cleland TA (2014) Construction of odor representations by olfactory bulb microcircuits. Prog Brain Res 208:177–203
9. Cleland TA, Sethupathy P (2006) Non-topographical contrast enhancement in the olfactory bulb. BMC Neurosci 7:7

10. Mandairon N, Ferretti CJ, Stack CM, Rubin DB, Cleland TA, Linster C (2006) Cholinergic modulation in the olfactory bulb influences spontaneous olfactory discrimination in adult rats. Eur J Neurosci 24:3234–3244
11. Cleland TA, Chen S-YT, Hozer KW, Ukatu HN, Wong KJ, Zheng F (2012) Sequential mechanisms underlying concentration invariance in biological olfaction. Front Neuroeng 4:21
12. Banerjee A, Marbach F, Anselmi F, Koh MS, Davis MB, Garcia da Silva P, Delevich K, Oyibo HK, Gupta P, Li B, Albeanu DF (2015) An interglomerular circuit gates glomerular output and implements gain control in the mouse olfactory bulb. Neuron 87:193–207
13. Igarashi KM, Ieki N, An M, Yamaguchi Y, Nagayama S, Kobayakawa K, Kobayakawa R, Tanifuji M, Sakano H, Chen WR, Mori K (2012) Parallel mitral and tufted cell pathways route distinct odor information to different targets in the olfactory cortex. J Neurosci 32:7970–7985
14. Fantana AL, Soucy ER, Meister M (2008) Rat olfactory bulb mitral cells receive sparse glomerular inputs. Neuron 59:802–814
15. Lepousez G, Nissant A, Bryant AK, Gheusi G, Greer CA, Lledo PM (2014) Olfactory learning promotes input-specific synaptic plasticity in adult-born neurons. Proc Natl Acad Sci U S A 111:13984–13989
16. Mandairon N, Linster C (2009) Odor perception and olfactory bulb plasticity in adult mammals. J Neurophysiol 101:2204–2209
17. Pressler RT, Inoue T, Strowbridge BW (2007) Muscarinic receptor activation modulates granule cell excitability and potentiates inhibition onto mitral cells in the rat olfactory bulb. J Neurosci 27:10969–10981
18. Inoue T, Strowbridge BW (2008) Transient activity induces a long-lasting increase in the excitability of olfactory bulb interneurons. J Neurophysiol 99:187–199
19. Li G, Cleland TA (2013) A two-layer biophysical model of cholinergic neuromodulation in olfactory bulb. J Neurosci 33:3037–3058
20. Rall W, Shepherd GM (1968) Theoretical reconstruction of field potentials and dendrodendritic synaptic interactions in olfactory bulb. J Neurophysiol 31:884–915
21. Lagier S, Carleton A, Lledo P-M (2004) Interplay between local GABAergic interneurons and relay neurons generates gamma oscillations in the rat olfactory bulb. J Neurosci 24:4382–4392
22. Neville KR, Haberly LB (2003) Beta and gamma oscillations in the olfactory system of the urethane-anesthetized rat. J Neurophysiol 90:3921–3930
23. Schoppa NE (2006) Synchronization of olfactory bulb mitral cells by precisely timed inhibitory inputs. Neuron 49:271–283
24. Schoppa NE (2006) AMPA/kainate receptors drive rapid output and precise synchrony in olfactory bulb granule cells. J Neurosci 26:12996–13006
25. Desmaisons D, Vincent JD, Lledo PM (1999) Control of action potential timing by intrinsic subthreshold oscillations in olfactory bulb output neurons. J Neurosci 19:10727–10737
26. Li G, Cleland TA (2017) A coupled-oscillator model of olfactory bulb gamma oscillations. PLoS Comput Biol 13(11):e1005760
27. David F, Courtiol E, Buonviso N, Fourcaud-Trocmé N (2015) Competing mechanisms of gamma and beta oscillations in the olfactory bulb based on multimodal inhibition of mitral cells over a respiratory cycle. eNeuro 2. https://doi.org/10.1523/ENEURO.0018-15.2015
28. Osinski BL, Kay LM (2016) Granule cell excitability mediates gamma and beta oscillations in a model of the dendrodendritic microcircuit. J Neurophysiol 116:522–539
29. Hayar A, Karnup S, Shipley MT, Ennis M (2004) Olfactory bulb glomeruli: external tufted cells intrinsically burst at theta frequency and are entrained by patterned olfactory input. J Neurosci 24:1190–1199
30. Hayar A, Karnup S, Ennis M, Shipley MT (2004) External tufted cells: a major excitatory element that coordinates glomerular activity. J Neurosci 24:6676–6685
31. Najac M, De Saint Jan D, Reguero L, Grandes P, Charpak S (2011) Monosynaptic and polysynaptic feed-forward inputs to mitral cells from olfactory sensory neurons. J Neurosci 31:8722–8729
32. Gire DH, Franks KM, Zak JD, Tanaka KF, Whitesell JD, Mulligan AA, Hen R, Schoppa NE (2012) Mitral cells in the olfactory bulb are mainly excited through a multistep signaling path. J Neurosci 32:2964–2975
33. Marr D, Poggio T (1977) From understanding computation to understanding neural circuitry. Neurosciences Res Prog Bull 15:470–488
34. Harrison TA, Scott JW (1986) Olfactory bulb responses to odor stimulation: analysis of response pattern and intensity relationships. J Neurophysiol 56:1571–1589
35. Wellis DP, Scott JW, Harrison TA (1989) Discrimination among odorants by single neurons of the rat olfactory bulb. J Neurophysiol 61:1161–1177

36. Meredith M (1986) Patterned response to odor in mammalian olfactory bulb: the influence of intensity. J Neurophysiol 56:572–597
37. Aungst JL, Heyward PM, Puche AC, Karnup SV, Hayar A, Szabo G, Shipley MT (2003) Centre-surround inhibition among olfactory bulb glomeruli. Nature 426:623–629
38. Cleland TA, Johnson BA, Leon M, Linster C (2007) Relational representation in the olfactory system. Proc Natl Acad Sci U S A 104:1953–1958
39. Koch C (1998) Biophysics of computation: information processing in single neurons. Oxford University Press, New York
40. Koch C, Segev I (eds) (1999) Methods in neuronal modeling: from ions to networks. Bradford, Cambridge, MA
41. Gerstner W, Kistler WM, Naud R, Paninski L (2014) Neuronal dynamics: from single neurons to networks and models of cognition. Cambridge University Press, Cambridge
42. Rubin DB, Cleland TA (2006) Dynamical mechanisms of odor processing in olfactory bulb mitral cells. J Neurophysiol 96:555–568
43. Sethupathy P, Rubin DB, Li G, Cleland TA (2013) A model of electrophysiological heterogeneity in periglomerular cells. Front Comput Neurosci 7:49
44. Rall W (1959) Branching dendritic trees and motoneuron membrane resistivity. Exp Neurol 1:491–527
45. Hodgkin AL, Huxley AF (1952) A quantitative description of membrane current and its application to conduction and excitation in nerve. J Physiol 117:500–544
46. Peace ST, Johnson BC, Li G, Kaiser M, Fukunaga I, Schaefer AT, Molnar AC, Cleland TA (2017) Coherent olfactory bulb gamma oscillations arise from coupling independent columnar oscillators. BioRxiv. https://doi.org/10.1101/213827
47. Shen GY, Chen WR, Midtgaard J, Shepherd GM, Hines ML (1999) Computational analysis of action potential initiation in mitral cell soma and dendrites based on dual patch recordings. J Neurophysiol 82:3006–3020
48. Chen WR, Shepherd GM (1997) Membrane and synaptic properties of mitral cells in slices of rat olfactory bulb. Brain Res 745:189–196
49. Xiong W, Chen WR (2002) Dynamic gating of spike propagation in the mitral cell lateral dendrites. Neuron 34:115–126
50. Bhalla US, Bower JM (1993) Exploring parameter space in detailed single neuron models: simulations of the mitral and granule cells of the olfactory bulb. J Neurophysiol 69:1948–1965
51. Davison AP, Feng J, Brown D (2000) A reduced compartmental model of the mitral cell for use in network models of the olfactory bulb. Brain Res Bull 51:393–399
52. Bathellier B, Lagier S, Faure P, Lledo P-M (2006) Circuit properties generating gamma oscillations in a network model of the olfactory bulb. J Neurophysiol 95:2678–2691
53. Brea JN, Kay LM, Kopell NJ (2009) Biophysical model for gamma rhythms in the olfactory bulb via subthreshold oscillations. Proc Natl Acad Sci U S A 106:21954–21959
54. Shao Z, Puche AC, Kiyokage E, Szabo G, Shipley MT (2009) Two GABAergic intraglomerular circuits differentially regulate tonic and phasic presynaptic inhibition of olfactory nerve terminals. J Neurophysiol 101:1988–2001
55. McQuiston AR, Katz LC (2001) Electrophysiology of interneurons in the glomerular layer of the rat olfactory bulb. J Neurophysiol 86:1899–1907
56. Kosaka K, Kosaka T (2005) Synaptic organization of the glomerulus in the main olfactory bulb: compartments of the glomerulus and heterogeneity of the periglomerular cells. Anat Sci Int 80:80–90
57. Kosaka K, Kosaka T (2007) Chemical properties of type 1 and type 2 periglomerular cells in the mouse olfactory bulb are different from those in the rat olfactory bulb. Brain Res 1167:42–55
58. Kiyokage E, Pan YZ, Shao Z, Kobayashi K, Szabo G, Yanagawa Y, Obata K, Okano H, Toida K, Puche AC, Shipley MT (2010) Molecular identity of periglomerular and short axon cells. J Neurosci 30:1185–1196
59. Isaacson JS, Strowbridge BW (1998) Olfactory reciprocal synapses: dendritic signaling in the CNS. Neuron 20:749–761
60. Cang J, Isaacson JS (2003) In vivo whole-cell recording of odor-evoked synaptic transmission in the rat olfactory bulb. J Neurosci 23:4108–4116
61. Pinato G, Midtgaard J (2003) Regulation of granule cell excitability by a low-threshold calcium spike in turtle olfactory bulb. J Neurophysiol 90:3341–3351
62. Balu R, Larimer P, Strowbridge BW (2004) Phasic stimuli evoke precisely timed spikes in intermittently discharging mitral cells. J Neurophysiol 92:743–753
63. Cadetti L, Belluzzi O (2001) Hyperpolarisation-activated current in glomerular cells of the rat olfactory bulb. Neuroreport 12:3117–3120
64. Le Jeune H, Aubert I, Jourdan F, Quirion R (1995) Comparative laminar distribution of

various autoradiographic cholinergic markers in adult main olfactory bulb. J Chem Neuroanat 9:99–112

65. Schoppa NE, Westbrook GL (1999) Regulation of synaptic timing in the olfactory bulb by an A-type potassium current. Nat Neurosci 2:1106–1113
66. Carnevale NT, Hines ML (2006) The neuron book. Cambridge University Press, Cambridge
67. Bower JM, Beeman D (2003) The book of GENESIS: exploring realistic neural models with the GEneral NEural SImulation System, Internet edition. http://www.genesis-sim.org/GENESIS.
68. Ray S, Bhalla US (2008) PyMOOSE: interoperable scripting in Python for MOOSE. Front Neuroinform 2:6
69. Vanier MC, Bower JM (1999) A comparative survey of automated parameter-search methods for compartmental neural models. J Comput Neurosci 7:149–171
70. Druckmann S, Banitt Y, Gidon A, Schurmann F, Markram H, Segev I (2007) A novel multiple objective optimization framework for constraining conductance-based neuron models by experimental data. Front Neurosci 1:7–18
71. Rall W (1967) Distinguishing theoretical synaptic potentials computed for different soma-dendritic distributions of synaptic input. J Neurophysiol 30:1138–1168
72. Jack JJB, Noble D, Tsien RW (1975) Electric current flow in excitable cells. Clarendon Oxford, Oxford, UK
73. Destexhe A, Mainen ZF, Sejnowski TJ (1994) An efficient method for computing synaptic conductances based on a kinetic model of receptor binding. Neural Comput 6:14–18
74. Wang XJ, Buzsáki G (1996) Gamma oscillation by synaptic inhibition in a hippocampal interneuronal network model. J Neurosci 16:6402–6413
75. Huang L, Ung K, Garcia I, Quast KB, Cordiner K, Saggau P, Arenkiel BR (2016) Task learning promotes plasticity of interneuron connectivity maps in the olfactory bulb. J Neurosci 36:8856–8871
76. Moreno MM, Bath K, Kuczewski N, Sacquet J, Didier A, Mandairon N (2012) Action of the noradrenergic system on adult-born cells is required for olfactory perceptual learning. J Neurosci 32:3748–3758
77. Gheusi G, Lledo PM (2014) Adult neurogenesis in the olfactory system shapes odor memory and perception. Prog Brain Res 208:157–175
78. Beshel J, Kopell N, Kay LM (2007) Olfactory bulb gamma oscillations are enhanced with task demands. J Neurosci 27:8358–8365
79. Doucette W, Restrepo D (2008) Profound context-dependent plasticity of mitral cell responses in olfactory bulb. PLoS Biol 6:e258